10-8-2019

LiGaOS is a Fast Li-Ion Conductor: a First-Principles Prediction

Xueling Lei

Wenjun Wu

Bo Xu

Chuying Ouyang

Kevin Huang
University of South Carolina - Columbia, huang46@cec.sc.edu

Publication Info

Published in *Materials & Design*, Volume 185, 2019.

Materials & Design 185 (2020) 108264

Contents lists available at ScienceDirect

Materials & Design

journal homepage: www.elsevier.com/locate/matdes

LiGaOS is a fast Li-Ion conductor: A first-principles prediction

Xueling Lei [a, *], Wenjun Wu [a], Bo Xu [a], Chuying Ouyang [a], Kevin Huang [b, **]

[a] Department of Physics, Laboratory of Computational Materials Physics, Jiangxi Normal University, Nanchang, Jiangxi, 330022, China
[b] Department of Mechanical Engineering, University of South Carolina, Columbia, SC, 29201, USA

HIGHLIGHTS

- The structural stability and Li-ion diffusion in the LiGaOS crystal were studied by first-principles calculations.
- LiGaOS has wide electrochemical window of 5.44 eV and high ionic conductivity of 10^{-3} cm^2/s at room temperature.
- The "kick-off" collective migration is dominant mechanism, the interstitial Li direct migration is a secondary mechanism.

GRAPHICAL ABSTRACT

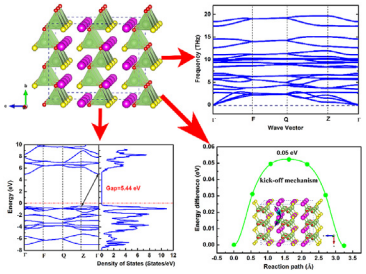

ARTICLE INFO

Article history:
Received 19 June 2019
Received in revised form
7 October 2019
Accepted 8 October 2019
Available online 10 October 2019

Keywords:
Superionic conductor
First-principles
Li interstitial
"Kick-off" mechanism

ABSTRACT

Solid Li-ion conducting electrolytes are highly sought for all solid-state Li-batteries, which are considered the next-generation safe batteries. Here a systematic computational study on the intrinsic transport properties of lithium gallium oxysulfide, LiGaOS (S. G. $Pmc2_1$), as a potential solid-state Li-ion electrolyte have been reported. The phonon dispersion spectrum analysis indicates that LiGaOS crystal structure is dynamically stable. The energy band structure and density of states calculations suggest that LiGaOS is an insulator with a wide indirect band gap of ~5.44 eV. The CI-NEB calculations reveal that the "kick-off" collective migration via Li-interstitials is the dominant conduction mechanism for Li-transport, with an extremely low energy barrier of 0.05 eV. The corresponding Li-ion self-diffusion coefficient estimated by transition state theory is in the order of magnitude of 10^{-3} cm^2/s at room temperature, with the dominant charge carrier being Li-interstitial. Overall, the presented first-principles calculations suggest that LiGaOS is a promising solid Li-ion electrolyte for future all-solid-state lithium batteries.

1. Introduction

The use of organics-based liquid electrolytes enables the benchmark Li-ion batteries (LIBs) to operate at high voltage (~3 V), a significant advantage over conventional 1.5 V aqueous batteries. However, these organic electrolytes are flammable in nature, overheating of which, for example by a faster charging/discharging rate, can ignite fire and cause thermal runaways that have been a serious safety concern on applications [1]. To fundamentally solve this safety problem, the electrolyte needs to be changed to a nonflammable solid material that not only conducts Li-ion well, but also are chemically compatible with the adjacent electrodes and electrochemically stable within a wide working voltage window.

So far, good solid-state Li-ion conductors are mainly found in a limited group of materials [2–4]. A well-known group is $Li_{10}GeP_2S_{12}$ (LGPS) [5] and its derivatives $Li_{10}MP_2X_{12}$ (M = Ge, Sn, Si, …; X = S, Se, …) [6,7] and $Li_7P_3S_{11}$ glass ceramics [8]. LGPS and its derivatives generally have a high Li-ion conductivity, *e.g.* 1.2×10^{-2} S/cm at room temperature, but they are air/moisture-

* Corresponding author.
** Corresponding author.
E-mail addresses: xueling@mail.ustc.edu.cn (X. Lei), HUANG46@cec.sc.edu (K. Huang).

https://doi.org/10.1016/j.matdes.2019.108264

sensitive and electrochemically unstable at both low and high potentials due to Li-reduction and Li-extraction, respectively [9,10]. Most recently, Yu et al. [11] reported a diffusion coefficient of $1.70(3) \times 10^{-14}$ cm^2/s at 333 K and an energy barrier of 0.132 eV for the Li-ion transport between Li_2S cathode and $Li_7P_3S_{11}$ electrolyte, the small diffusion coefficient suggests that these contact interfaces between electrode and electrolyte are relatively scarce. Another widely studied family of solid-state Li-ion conductors is garnet-structured Li-containing oxides, among which the cubic phase $Li_7La_3Zr_2O_{12}$ (LLZO) is widely studied. The LLZO exhibits a Li-ion conductivity of 2.6×10^{-4} S/cm at room temperature [12], and has a sufficiently large band gap (~6.4 eV) to ensure a good electrochemical stability even with Li-metal as an anode [13]. In addition, the total ionic conductivity can be enhanced to 1.41×10^{-4} Scm^{-1} at 30 °C and 5.2×10^{-4} Scm^{-1} at room temperature via Al doping and Ca doping, respectively [14,15]. Most recently, it was reported that Nb–Gd co-doping LLZO electrolyte ($Li_{6.5}La_3Zr_{1.3}Nb_{0.6}Gd_{0.1}O_{12}$) presented the high Li-ion conductivity of 9.86×10^{-4} Scm^{-1} when sintered at 1150 °C for 12 h [16]. Also, the mechanical strength and ionic conductivity of Ta-doped LLZO solid electrolyte ($Li_{6.4}La_3Zr_{1.4}Ta_{0.6}O_{12}$) have been enhanced at room temperature by oscillatory pressure sintering technique [17]. Recently, a lithium-rich antiperovskite material Li_3OCl has also been reported as a promising Li-ion conductor with an ionic conductivity greater than 10^{-3} S/cm at room temperature [18]. Following this work, we performed a first-principles calculation, revealing that Li_3OCl has a wide band gap of 6.26 eV, similar to LLZO [19].

Throughout the history of solid state ionics, it is fair to say that discovery of new solid-state ionic conductors is a very challenging task. Therefore, materials design through computational science becomes more and more important in finding new solid-state Li-ion conductors. Recently, based on the crystal structure prediction method, Xiao et al. [20] theoretically design two kinds of AlS_2O_2-layer stacking structures: *Pmc*2$_1$ and *Cmc*2$_1$ with a chemical composition of LiAlOS, and predict it to be a potential Li-ion conductor. The materials' band gap reported is 5.6 eV, and the Li-ion migration barrier is less than 50 meV with a Li-interstitial based "kick-off" migration mechanism. This is an excellent attempt to computationally design a new solid-state Li-ion conductor, which may pave the way to discover more new electrochemical materials in the future. Inspired by the fact that Ga and Al belong to the same main III group with similar physicochemical properties, we naturally wonder whether LiGaOS can also be a good Li-ion conductor, and if LiMSO (M = Al, Ga, In) represents a new family of high-conductivity Li-ion conductors.

In the present work, a suite of systematic first-principles calculations on the intrinsic transport properties of LiGaOS crystal in *Pmc*2$_1$ symmetry, including structural stability, electronic property, defect structure, and Li-ion self-diffusion have been performed. The Li-ion migration mechanisms with different point defects are particularly examined in detail. In addition, the effect of temperature for Li-ion migration is also investigated using the first-principles molecular dynamics (FPMD) method. We expect that the results offered by the current study will provide critical insights for discovery of new solid-state Li-ion electrolytes much needed for high-energy-density and safe all-solid-state lithium metal batteries (LMBs) in the future.

2. Computational details and models

All the calculations in the present work were performed using the VASP code [21,22]. The projected augmented wave (PAW) to describe the valence electron and core-ion interactions [23,24] and the GGA/PBE exchange–correlation functional [25] to calculate the electron exchange and correlation energies were used. A cutoff energy of 500 eV was applied to the plane wave basis expansion. The electronic structures were calculated using a primitive cell with 8 atoms and a $6 \times 4 \times 4$ Monkhorst–Pack [26] k-point grid in the first Brillouin zone. The Li-ion self-diffusion was calculated on a $3 \times 2 \times 2$ supercell with 96 atoms using the climbing image nudged elastic band (CI-NEB) method [27,28] to seek for the saddle points and minimum energy paths. Correspondingly, a small $2 \times 2 \times 2$ Monkhorst–Pack k-point grid was used for the integration over the first Brillouin zone. The lattice parameters and ionic positions were fully relaxed until the total energies and ionic forces were less than 10^{-5} eV and 0.01 eVÅ^{-1}, respectively.

For phonon dispersion spectrum calculations, the PHONOPY code was used [29], which directly uses the dynamic matrices calculated by the density functional perturbation theory (DFPT) [30] implemented in VASP. A $6 \times 4 \times 4$ k-point grid and 10^{-8} eV/Å electronic forces convergence were used.

For the FPMD simulations, the canonical ensemble (NVT) was employed. A Verlet algorithm was integrated with Newton's equations of motion at 300 K for 3 ps with a time step of 1 fs. The frequency of the temperature oscillations was controlled by the Nosé mass during the simulations. Additionally, a supercell of $3 \times 2 \times 2$ primitive cell (96 atoms) was used with a $1 \times 1 \times 1$ k-point sampling at the Γ-point.

3. Results and discussions

3.1. Crystal structure and stability

Here, the LiGaOS crystal structure with orthorhombic space group *Pmc*2$_1$ has been constructed, where Li, Ga, S and O atoms occupy Wyckoff positions at 2a, 2b, 2a, and 2b, respectively. In addition, it is noted that the structure of LiGaOS is not a sulfur-substituted version of $LiGaO_2$. $LiGaO_2$ crystal structure with space group of *Pna*21 has different symmetry from LiGaOS. The relaxed crystal structure of LiGaOS is shown in Fig. 1 (a), from which one can see that each Li or Ga atom coordinates with two O atoms and two S atoms, forming a tetrahedron. Like the structure of LiAlOS, GaS_2O_2 tetrahedra are connected to each other by sharing corners to form layers in the *ab* plane. The GaS_2O_2 planes constitute layer-by-layer stacking along the *c* direction separated by severely distorted LiS_2O_2 tetrahedra. The lattice parameters are $a = 3.587$ Å, $b = 6.514$ Å, and $c = 5.456$ Å, which are slightly larger than those of LiAlOS [20]. This can be explained by the larger ionic radius of Ga than that of Al. The relaxed Ga–S and Ga–O distances are 2.272 Å and 1.886 Å, respectively, which are larger than Al–S and Al–O distances in oxysulfide LiAlSO [20]. On the contrary, the lengths of Li–S and Li–O bonds are 2.505 Å and 2.072 Å, respectively, which are 2.8% and 3.5% smaller than those in LiAlOS [20].

To evaluate the thermodynamic stability of the crystal structure determined above, the typical decomposition reactions of $LiGaOS \rightarrow 0.25Li_2O + 0.25Li_2S + 0.25Ga_2O_3 + 0.25Ga_2S_3$ and $LiGaOS \rightarrow 0.5LiGaO_2 + 0.5LiGaS_2$ have been taken into account. The related structures are taken from the Open Quantum Materials Database (OQMD) [31,32]. The reaction energies are calculated by the formulas

$$\Delta E = \frac{1}{4}\left(E_{Li_2O} + E_{Li_2S} + E_{Ga_2O_3} + E_{Ga_2S_3}\right) - E_{LiGaOS} \quad (1)$$

and

$$\Delta E = \frac{1}{2}\left(E_{LiGaO_2} + E_{LiGaS_2}\right) - E_{LiGaOS} \quad (2)$$

where E_{Li_2O}, E_{Li_2S}, $E_{Ga_2O_3}$, $E_{Ga_2S_3}$, E_{LiGaO_2}, E_{LiGaS_2} and E_{LiGaOS} are the total energy of optimized primitive cell of Li_2O, Li_2S, Ga_2O_3, Ga_2S_3,

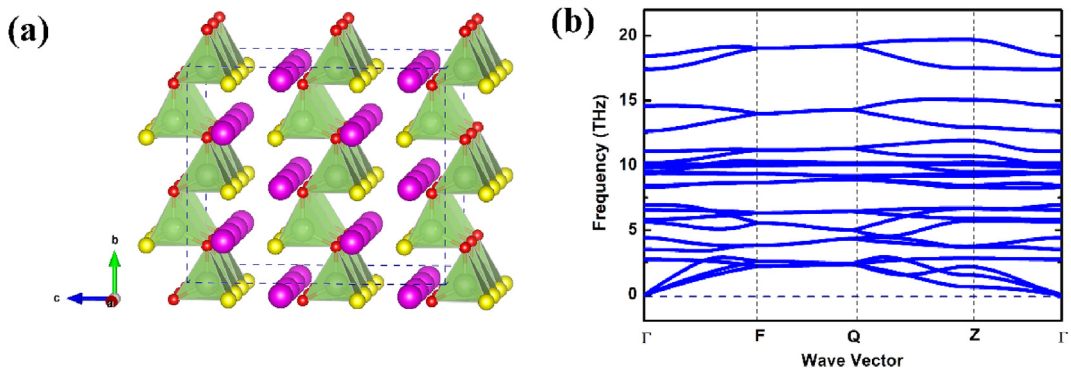

Fig. 1. Crystal structure of *Pmc2₁* LiGaOS, the red, yellow, purple, and green represent O, S, Li, and Ga atoms, respectively (a) and the phonon dispersion spectrum (b).

$LiGaO_2$, $LiGaS_2$ and LiGaOS crystal structures, respectively. The evaluated reaction energy is about 0.233 eV/atom for Eq. (1), indicating that it is possible to stabilize LiGaOS and to synthesize it from the parent phase. However, the calculated reaction energy of Eq. (2) is about −0.062 eV/atom, indicating that the predicted LiGaOS phase is thermodynamically unstable at 0 K with respect to $LiGaO_2$ and $LiGaS_2$. Nevertheless, the reaction energy of LiGaOS decomposed into $LiGaO_2$ and $LiGaS_2$ competing phase is relatively low, suggesting that it can exist as a metastable structure or be stabilized by entropic effects, as the newly predicted Li superionic conductor LiAlSO [20].

In general, the phonon dispersion spectrum could provide evidence for the crystal structure stability. The positive phonon frequencies indicate a stable crystal, while the imaginary frequencies indicate otherwise. To verify the stability of LiGaOS crystal, its phonon dispersion spectrum are examined and the results are shown in Fig. 1 (b). There are eight atoms in our simulated primitive cell, producing three acoustic branches and twenty-one optical branches in the dispersion curves. Fig. 1 (b) shows that phonon frequencies of LiGaOS crystal are all positive, suggesting that LiGaOS crystal structure is dynamically stable.

3.2. Electronic property

For an electrolyte material, it is required that it be a pure ionic conductor with negligible electronic conductivity. This is to say that the electrolyte material must have an adequate band gap to ensure electronic structural stability and to prevent electronic leakage. To examine the electronic structure of LiGaOS, the energy band structure and density of states (DOS) of ground state in LiGaOS are calculated. Since the GGA-PBE function usually underestimates band gap, herein the high-level HSE06 approach are employed to accessing the band gap [33]. Fig. 2 shows that LiGaOS has an indirect band gap of ~5.44 eV with the conduction band minimum (CBM) and valence band maximum (VBM) located at the Γ and Z points of the first Brillouin zone, respectively. The large band gap implies that LiGaOS is an insulator with negligible electronic conductivity, which can ensure a wide electrochemical window.

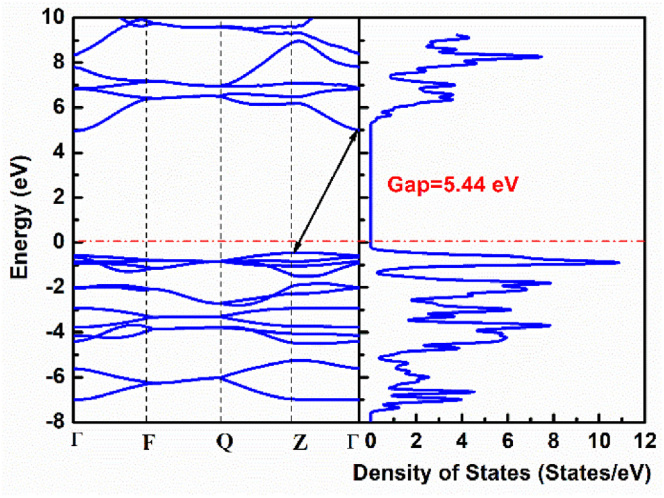

Fig. 2. Density of states (DOS) and the band structure of *Pmc2₁* LiGaOS.

3.3. Li-ion self-diffusion in LiGaOS

3.3.1. Defect structure and formation energy

Generally, Li-ion conductivity depends on the concentration of charge carriers and energy barrier to migration of charge carriers. The types of defects as a charge carrier as well as their concentrations are important factors determining the diffusion coefficient and thus conductivity. Therefore, the types of defects have been first studied. Since point defects are the most common defects in solid materials, here four types of point defects represented by Kröger-Vink notations are considered: isolated charged point defects including Li-vacancy (V'_{Li}) and interstitial-Li ($Li^{\bullet}_{i}$) and charge neutral point-defect clusters including Frenkel defect pair ($V'_{Li} - Li^{\bullet}_{i}$) and Li_2O Schottky defect pair ($2V'_{Li} - V^{\bullet\bullet}_{O}$). The Li-vacancy can be created by removing one Li-ion from its lattice site in the perfect system, and the interstitial-Li defect is created by adding one Li-ion into the interstitial site in the perfect system. The Frenkel defect pair is created by $Li^{\times}_{Li} \rightarrow V'_{Li} + Li^{\bullet}_{i}$, *i. e.* a Li at the lattice site is moved to the interstitial site in the perfect system, leaving behind a vacancy and forming ($V'_{Li} - Li^{\bullet}_{i}$) Frenkel defect pair. For Li_2O Schottky defect pair, it is created by $2Li^{\times}_{Li} + O^{\times}_{O} \rightarrow 2V'_{Li} + V^{\bullet\bullet}_{O} + Li_2O$, meaning that two Li-lattice sites and one O-lattice site are removed simultaneously, forming a ($2V'_{Li} - V^{\bullet\bullet}_{O}$) Li_2O Schottky defect pair.

Then the defect configurations and formation energies have been studied. Based on the symmetry of LiGaOS crystal structure, Fig. 3 (a) shows one created Li-vacancy defect and one created interstitial-Li defect in the structure, respectively. For the Frenkel defect pair, according to the distance between V'_{Li} and $Li^{\bullet}_{i}$, two different configurations: V_{near} and V_{far}, as indicated in Fig. 3(b) are considered; V_{near} represents V'_{Li} near $Li^{\bullet}_{i}$, while V_{far} represents V'_{Li} far from $Li^{\bullet}_{i}$. As for the Li_2O Schottky defect pair, two different defect configurations denoted by V_{concen} and $V_{disperse}$ are also considered, as shown in Fig. 3 (c) and 3 (d); V_{concen} represents the concentrated distribution of ($2V'_{Li} - V^{\bullet\bullet}_{O}$) defect pair, while $V_{disperse}$ represents the dispersed distribution of ($2V'_{Li} - V^{\bullet\bullet}_{O}$) defect pair.

In a solid material, the defect concentration is strongly related to the defect formation energy. Here, the defect formation energy are defined as $E_f = E_{defect} - E_{perfect} \pm u_i$, where E_{defect} and $E_{perfect}$ are the total energy with and without defect in the $3 \times 2 \times 2$ supercell, and

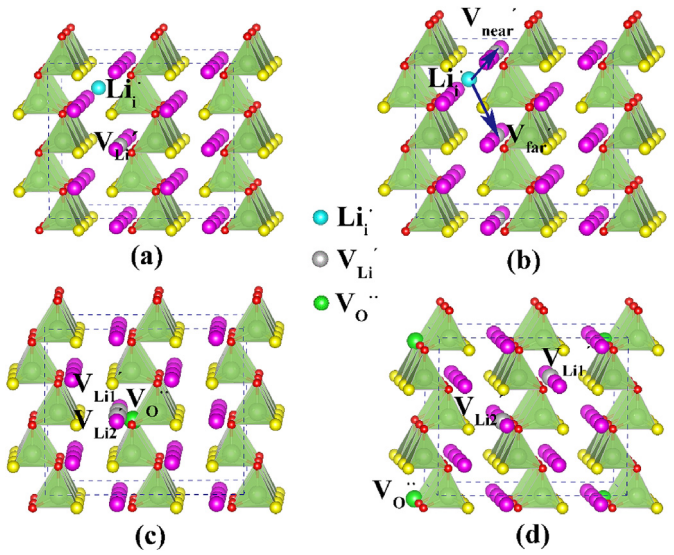

Fig. 3. Schematic representations of defect configurations in (a) single Li-vacancy ($\mathbf{V}'_{Li}$) and single interstitial-Li ($Li_i^{\cdot}$), (b) Frenkel defect pair ($\mathbf{V}'_{Li} - \mathbf{Li}_i^{\cdot}$), (c) concentrated distribution of Li_2O Schottky defect pair ($2\mathbf{V}'_{Li} - \mathbf{V}_O^{\cdot\cdot}$), and (d) dispersed distribution of Li_2O Schottky defect pair ($2\mathbf{V}'_{Li} - \mathbf{V}_O^{\cdot\cdot}$).

u_i is the chemical potential of Li or Li_2O compound calculated from the body centered cubic (bcc) Li metal and face centered cubic (fcc) Li_2O crystal structure. Based on the definition of the considered four types of defects, the calculated defect formation energies are listed in Table 1, from which one can see that the most stable defect configuration is V_{near} for ($V'_{Li} - Li_i^{\cdot}$) defect pair and V_{concen} for ($2V'_{Li} - V_O^{\cdot\cdot}$) defect pair, suggesting that the energy of a defect system increases with increasing distance between defects. This is a reasonable assertion given the coulombic attractions between V'_{Li} and $Li_i^{\cdot}$ and between V'_{Li} and $V_O^{\cdot\cdot}$. Furthermore, it is noted that the formation energies for single V'_{Li} and $Li_i^{\cdot}$ are roughly 4.01 eV and 0.70 eV, respectively, implying that the concentration of Li-vacancy should be very low at room temperature, and the most dominant defect is interstitial Li ($Li_i^{\cdot}$) in LiGaOS. On the other hand, the optimal defect formation energies for the charge neutral ($V'_{Li} - Li_i^{\cdot}$) Frenkel defect pair and ($2V'_{Li} - V_O^{\cdot\cdot}$) Schottky defect pair are 1.34 eV (0.67 eV per defect) and 3.45 eV (1.15 eV per defect), respectively. Therefore, the ($V'_{Li} - Li_i^{\cdot}$) Frenkel defect pair is presumably the predominant defect pair in LiGaOS at room temperature.

3.3.2. Li-migration via vacancy mechanism

Since the electronic structure in LiGaOS is suited for pure ionic conduction, how fast ionic charge carriers can migrate in LiGaOS becomes critical to the ultimate electrolyte conductivity. After the charge-carrier formation energies of V'_{Li}, $Li_i^{\cdot}$, ($V'_{Li} - Li_i^{\cdot}$) and ($2V'_{Li} - V_O^{\cdot\cdot}$) were studied, next the energy barriers of the charge carrier migration are evaluated. First, Li-vacancy migration in *Pmc2₁* LiGaOS are considered. We hypothesize that Li-vacancies directly hop between two neighboring Li sites. Fig. 4 shows the migration path and barriers of a single Li-vacancy migration along the *bc*-plane and *a*-axis in LiGaOS. From the symmetry of LiGaOS crystal structure, four possible migration pathways in the *bc*-plane are identified in Fig. 4 (a), denoted as P—I, P-II, P-III, and P-IV, and calculate the corresponding migration energy barriers in Fig. 4 (b). The results show that the lowest barrier is 1.14 eV, corresponding to the P—I and P-II pathways, and the highest barrier is 1.52 eV, corresponding to the P-III and P-IV pathways. Such higher energy barriers indicate that the Li-vacancy migration in the *bc*-plane is very difficult. For migration along the *a*-axis in LiGaOS, only one pathway is identified for Li-vacancy from the structural features of LiGaOS. Fig. 4 (c)—(d) show an energy barrier of 0.38 eV, which suggests that the Li-vacancy migration along *a*-direction is possible [34].

As discussed above in defect structure, we know that the Li-vacancy formation energy is quite high, while for the Frenkel defect pair it is much smaller. Therefore, the Li-vacancy migration in the case of the Frenkel defect pair are also examined. A possible low-energy migration pathway are created shown in Fig. 5 (a), and the corresponding energy profile for Li-vacancy migration is shown in Fig. 5 (b). It is evident that the migration pathway of Li-vacancy along *a*-axis follows: $V_1 \rightarrow V_2 \rightarrow V_3 \rightarrow V_1$, and the corresponding energy barrier is 0.49 eV, which is 0.11 eV higher than that of a single Li-vacancy migration. This may be due to the Coulombic attraction between Li-vacancy and interstitial Li, making a Li-vacancy leaving the host a little bit difficult.

According to the above discussion, we know that a single Li-vacancy migration energy barrier along the *a*-axis is low (0.38 eV), but the formation of single Li-vacancy is very difficult due to its high defect formation energy (4.01 eV). On the contrary, although the defect formation energy of Frenkel defect pair is low (0.67 eV per defect), the energy barrier of Li-vacancy migration in the case of Frenkel defect pair is relatively high (0.49 eV). Therefore, it is concluded that the contribution of charge carriers from Li-vacancy to the ionic conductivity of LiGaOS crystals cannot be significant.

3.3.3. Li migration via interstitial mechanism

Now we turn to interstitial-Li defect migration in *Pmc2₁* LiGaOS, including interstitial Li-defect direct migration mechanism and "kick-off" collective migration mechanism. Direct migration mechanism describes a direct hopping of interstitial Li between empty interstitial sites, while the "kick-off" collective migration mechanism describes an interstitial Li-defect pushes the adjacent lattice Li into the next interstitial site and occupies the lattice site by itself. Fig. 6 compares direct migration of the interstitial Li-defect along the *b*-axis and a "kick-off" collective migration along the *a*-axis in LiGaOS. For the direct migration mechanism, Fig. 6 (a)—(b), the interstitial Li1 migration from an interstitial site to its neighbor interstitial site need to overcome an energy barrier of 0.24 eV. In contrast, Fig. 6 (c)—(d) shows that the "kick-off" collective mechanism, involving interstitial Li1 migration from an interstitial site to the nearest lattice site and the lattice Li2 migration from the host lattice site to the next interstitial site, needs to overcome an energy barrier as low as 0.05 eV; this level of energy barriers is lower than many known Li-ion conductors [35—37]. Overall, it is envisioned that interstitial Li-defects migrate within a two-dimensional (2D) channel in the *ab* plane formed by corner-shared GaS_2O_2 tetrahedra and separated by Li atoms. The "kick-off" collective migration along the *a*-direction with a low energy barrier of 0.05 eV should be a dominant Li-transport mechanism, while the direct migration along the *b*-direction with an energy barrier of 0.24 eV is a secondary transport mechanism. As we know, the local environment of moving Li in the NEB calculation is complicated, including ionic valence, voids size, voids number and so on. Nevertheless, increasing the concentration of interstitial-Li defects is another key to achieve high Li-ion conductivity.

Table 1
Defect formation energy of single $\mathbf{V}'_{Li}$ and $\mathbf{Li}_i^{\cdot}$, ($\mathbf{V}'_{Li} - \mathbf{Li}_i^{\cdot}$) defect pairs $\mathbf{V_{near}}$ and $\mathbf{V_{far}}$, and ($2\mathbf{V}'_{Li} - \mathbf{V}_O^{\cdot\cdot}$) defect pairs $\mathbf{V_{concen}}$ and $\mathbf{V_{disperse}}$.

Defect type	V'_{Li}	$Li_i^{\cdot}$	V_{near}	V_{far}	V_{concen}	$V_{disperse}$
u_i(eV)	−1.91	−1.91	–	–	−14.35	−14.35
E_f(eV)	4.01	0.70	1.34	1.40	3.45	4.49

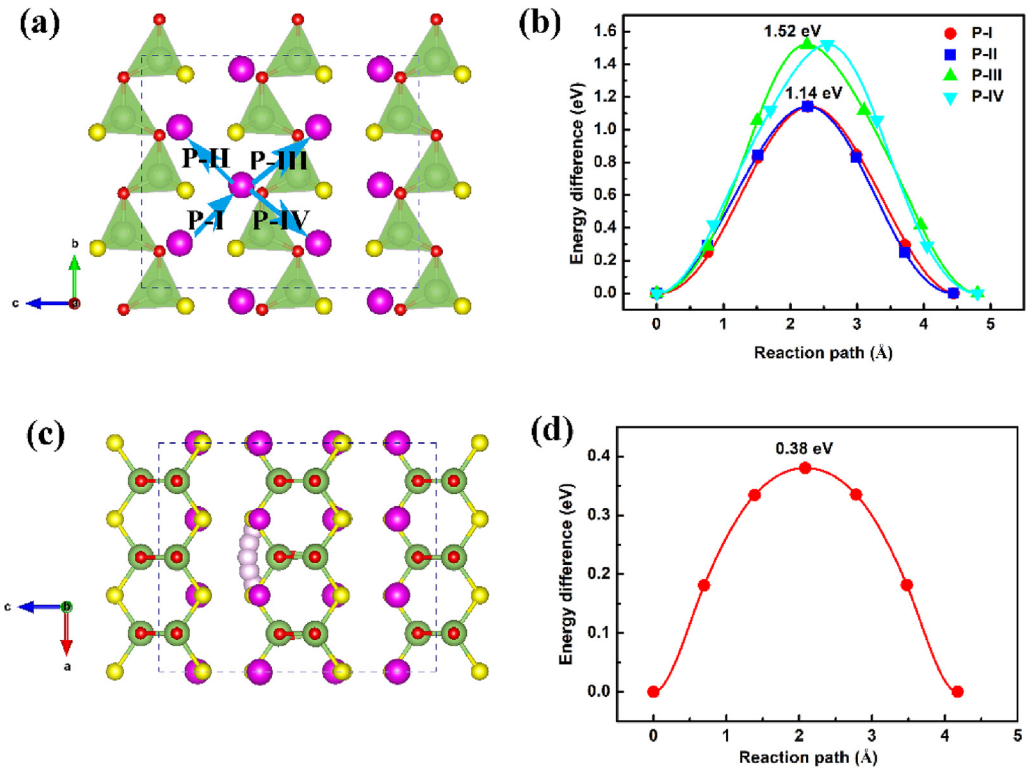

Fig. 4. Migration pathway and barriers for Li-vacancy migration along the *bc*-plane (a)–(b) and along the *a*-axis (c)–(d) in the $Pmc2_1$ LiGaOS.

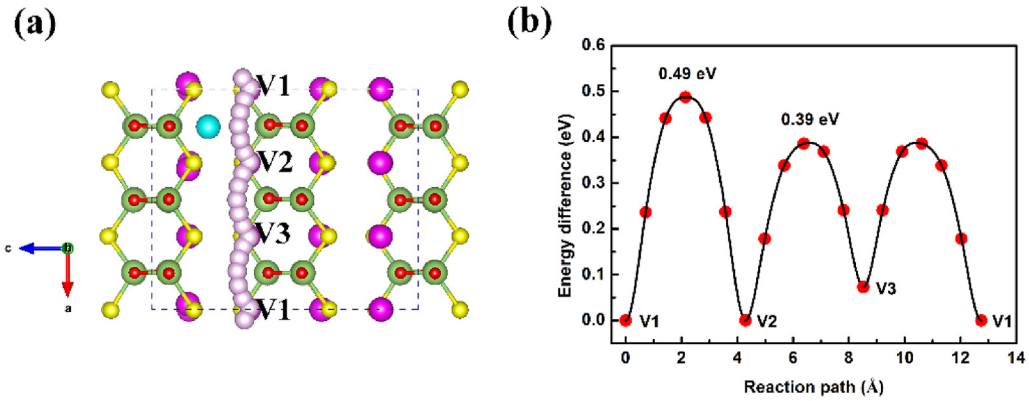

Fig. 5. The migration pathway (a) and energy profile (b) of Li-vacancy in the Frenkel defect pair. The blue ball represents the interstitial Li.

3.3.4. FPMD simulations of interstitial-Li migration via the "kick-off" mechanism

All the above calculations of Li-migration by CI-NEB method were conducted at 0 K. To learn about interstitial-Li migration in LiGaOS *vs* temperature, FPMD simulations under the Born Oppenheimer approximation are carried out. The simulations were performed at 300 K for 3000 fs. Fig. 7 shows a series of snapshots of "kick-off" collective migration along *x*-axis (or *a*-axis in the lattice coordinate) in the $Pmc2_1$ LiGaOS structure, which provides us a "live" picture to understand the mechanism of the "kick-off" collective migration. The big blue ball and brown ball, respectively, represent the interstitial Li and lattice Li in motion. The purple, red, yellow, and dark pink balls indicate the regular, immobile Li, O, S, and Ga atoms, respectively. Apparently, at the beginning, the blue ball is localized at an interstitial site, while other atoms are located at their respective lattice sites. Then, all atoms vibrate at their respective equilibrium positions with time before the "kick-off" collective migration kicks in. A positional comparison between interstitial Li and lattice Li in each snapshot shows that the interstitial Li moves to the nearest lattice site while the lattice Li simultaneously move to the next interstitial site, indicating a typical "kick-off" collective migration mechanism in the negative direction of the *x*-axis. Statistically speaking, the movement of interstitial Li to the positive or negative *x*-axis is random. More importantly, a complete "kick-off" migration process is observed to start in ~1900 fs and ends in ~2000 fs before the next "kick-off" migration step begins. The snapshots in 2060 fs and 2100 fs indicate the trajectory towards the beginning of the next-step "kick-off" migration. We also note, on the other hand, that other atoms such as regular Ga, S, O, and Li only vibrate with respect to their original equilibrium positions without any migration, and no breaking of Ga—S or Ga—O bonds is observed during the simulations. This again demonstrates that the LiGaOS structure with $Pmc2_1$ symmetry is thermodynamically stable at 300 K. In fact, we performed three MD simulations for the same structure at 300 K, one or two complete migration period can be observed in a supercell with one extra Li at

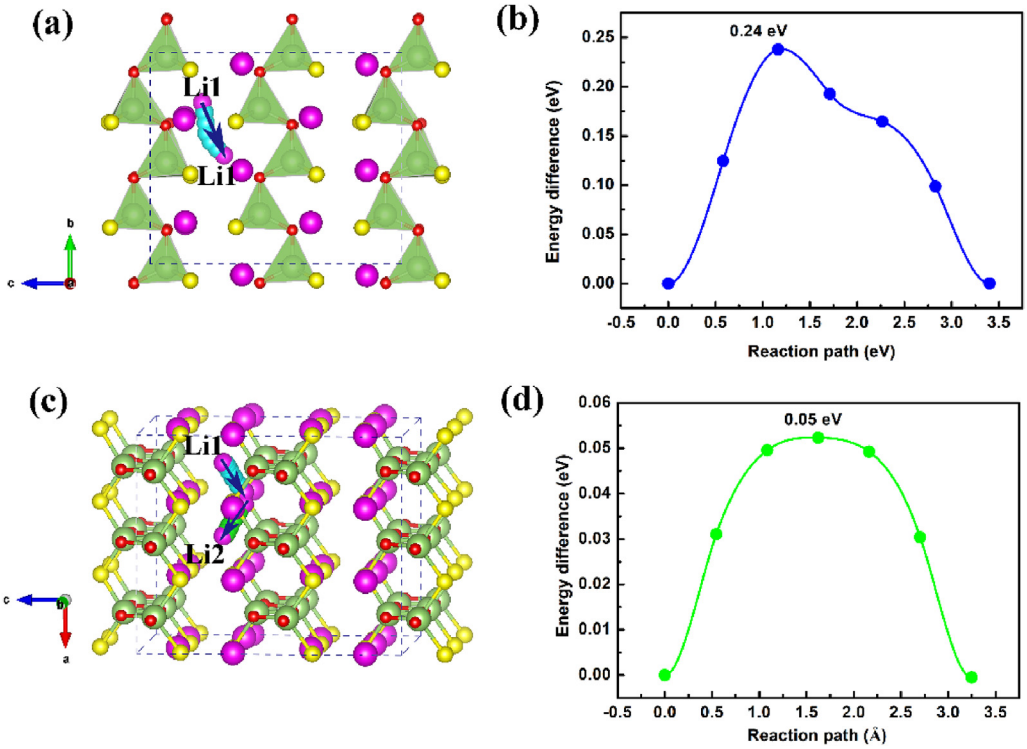

Fig. 6. Migration pathway and barriers for the direct interstitial Li-ion migration along the *b*-axis (a)–(b) and the "kick-off" collective migration along the *a*-axis (c)–(d) in the $Pmc2_1$ LiGaOS. Li1 and Li2 represent the interstitial Li and the lattice Li, respectively.

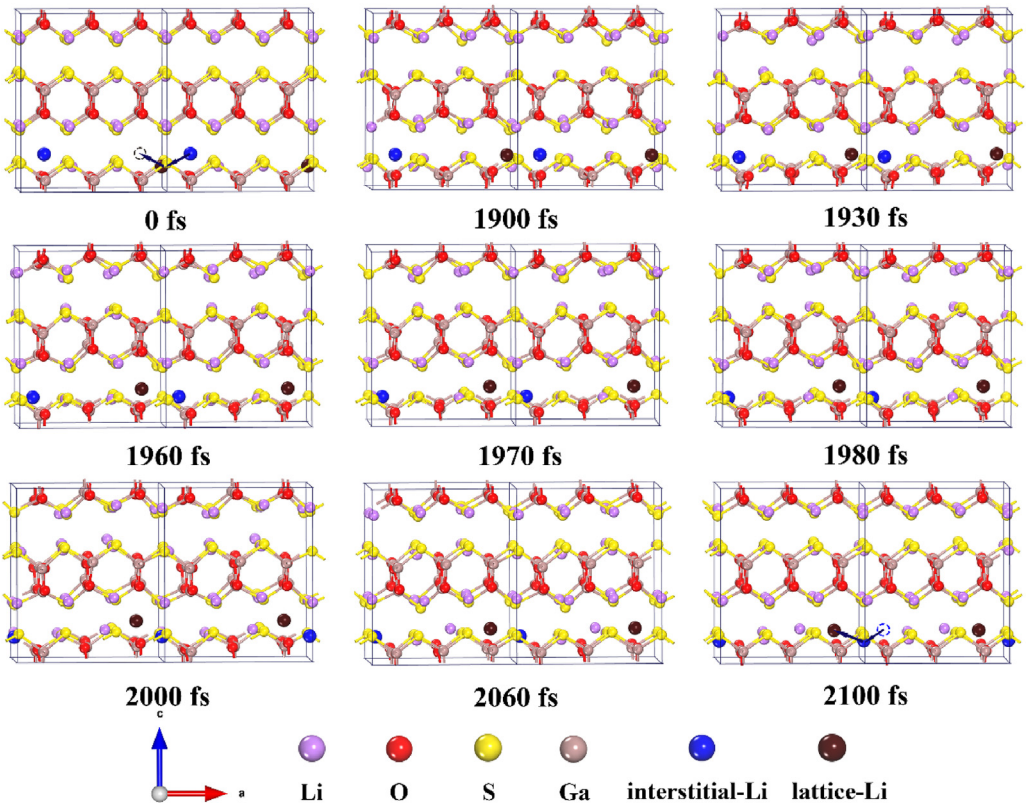

Fig. 7. Snapshots for the "kick-off" collective migration in the negative direction along the *a*-axis in the $Pmc2_1$ LiGaOS at 300 K for 3000 ps. The big blue ball and brown ball represent the interstitial Li and lattice Li in motion, respectively, and the arrows on the first and last snapshots show Li-ion migration direction.

the interstitial site in the 3000 fs simulations.

The corresponding trajectory of the interstitial Li and lattice Li together with their X and Z coordinates in the $Pmc2_1$ LiGaOS structure simulated at 300 K for 3000 fs are further shown in Fig. 8. From this simulation, it is evident that the trajectories of interstitial Li and lattice Li diffusion are 1D along the *x*-axis (*a*-direction in the lattice) with large displacements. Initially, the interstitial Li and lattice Li vibrate at their respective positions; then the interstitial Li hops to the nearest lattice site as evidenced by the decreasing of X and Z coordinates. Meanwhile, the lattice Li successfully jumps to the next interstitial site as evidenced by the decreasing of X coordinates and increasing of Z coordinates. Fig. 8 (c) shows the change of X and Z coordinates of the interstitial Li and lattice Li vs time. The decreasing of X coordinates and the intersection of Z coordinates again demonstrate that the "kick-off" migration takes place at ~ 1900 fs and completes at ~ 2000 fs. It is also evident from Fig. 8 (d) of MSDs that the instantaneous MSDs of regular Li, O, S, and Ga atoms are small constant values near zero and independent of time, implying that these atoms only vibrate at their lattice positions and are immobile throughout the simulation time. In contrast, MSDs of interstitial Li and lattice Li are first time independent, and then increase linearly with time, indicating that a simultaneous migration of interstitial Li and lattice Li begins after several vibrations at their equilibrium positions. The distinct features in Fig. 8 strongly suggests the possibility of the "kick-off" collective migration mechanism.

3.3.5. Li-ion self-diffusion coefficient

From the above results, we learn the migration pathway and energy barrier of Li-diffusion in the LiGaOS crystal and understand that the dominant Li-migration mechanism is "kick-off" collective migration. To facilitate a comparison of our findings with other Li-ion conductors, according to the transition state theory [38,39], the Li-ion self-diffusion coefficient are further estimated by $D = cd^2v \cdot \exp(-\Delta E/k_BT)$, where c, d, v, ΔE, k_B and T are pre-factor, Li-ion hopping distance, vibration frequency, migration energy barrier, Boltzmann constant, and absolute temperature, respectively, and v can be approximated as 10^{13} Hz based on our calculations for the phonon frequencies (see Fig. 1 b), c can be estimated by W/2 N, where W is the number of crystallographically similar nearest sites, and N is the dimension number of Li-ion diffusion. Moreover, the diffusion coefficient equation mentioned above is only valid for an uncorrelated random walk. With the calculated migration distance and energy barriers, D at room temperature ($T = 300$ K) can be estimated and the results are listed in Table 2. The Li-ion self-diffusion coefficient of ~10^{-3} cm^2/s at room temperature for the "kick-off" collective migration mechanism is at least one order of magnitude higher than that of Li self-diffusion along the *ab* plane in the P_1-LGPS [40].

In practice, one merit of solid electrolyte is the possibility of Li-metal anode design. To examine the stability of LiGaOS when in contact with Li metal, we think it needs to construct the interface model between lithium metal and LiGaOS and further more detailed studies should be carried out.

All in all, as far as we know, there is no experimental synthesis of LiGaOS so far. From the view point of calculation, we predict that LiGaOS has wide electrochemical window and high ionic conductivity, which is an ideal candidate for solid-state electrolyte of all-solid-state lithium batteries. We hope that our computational data can provide basic knowledge for experimental preparation of LiGaOS, and that LiGaOS can be synthesized experimentally in the

Table 2
Calculated migration distance (d), energy barriers (ΔE), and estimated Li-ion diffusion coefficients (D) at room temperature for four types of Li migration mechanism.

Migration mechanism	d(Å)	ΔE(eV)	D (cm^2/s)
V'_{Li}	3.68	0.38	10^{-8}
$V'_{Li} - Li^{\cdot}_i$	3.68	0.49	10^{-9}
$Li^{\cdot}_i$	2.95	0.24	10^{-6}
"kick-off"	1.99	0.05	10^{-3}

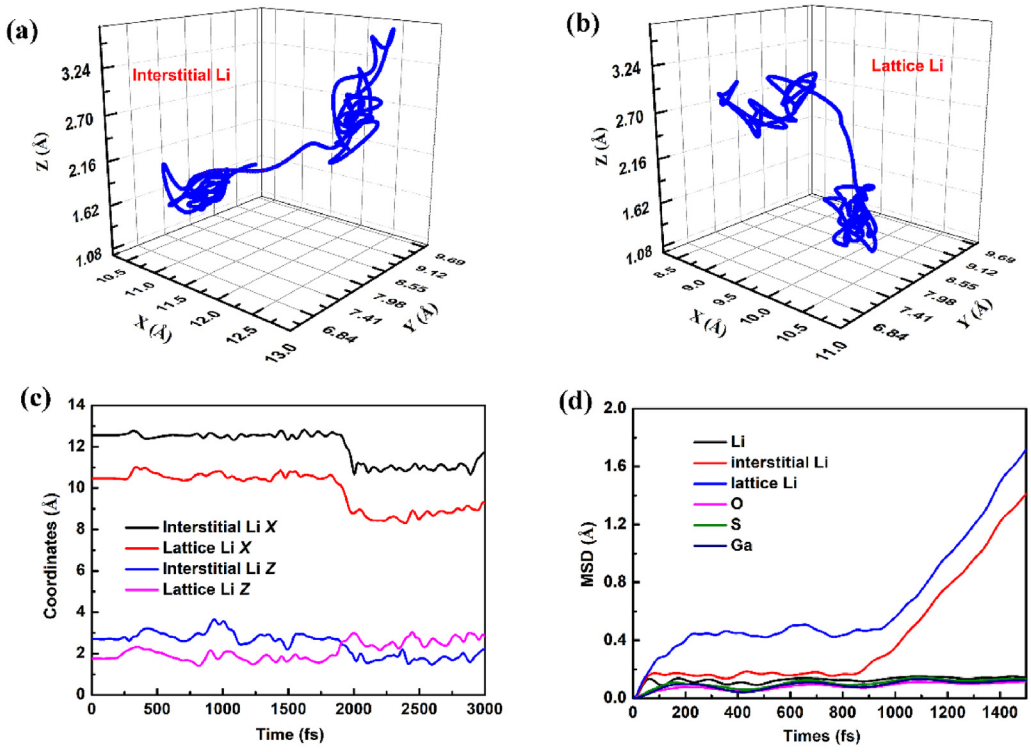

Fig. 8. Trajectories of the interstitial Li (a) and the lattice Li (b) along with their X and Z coordinates (c), and the MSD of regular Li, interstitial Li, lattice Li, regular O, S, and Ga atoms (d) in the $Pmc2_1$ LiGaOS simulated at 300 K for 3000 fs.

future.

4. Conclusions

In summary, through materials design, we identified a promising materials of fairly good Li-ion conductors, LiGaOS crystal. The crystal structure and stability, electronic properties, defect structure, and Li-ion migration mechanisms of oxysulfide LiGaOS have been systematically studied using first-principles calculations and FPMD simulations. The structure of LiGaOS in the *Pmc2₁* symmetry is like that of LiAlOS and composed of stacking layers of GaS_2O_2 tetrahedrons sharing vertex atoms with Li ions located between the layers. The phonon dispersion spectrum and FPMD simulations indicate that LiGaOS crystal structure is dynamically and thermodynamically stable. The electronic energy band structure and DOS calculations show that the *Pmc2₁* LiGaOS is an insulator with a wide indirect band gap of ~5.44 eV, which ensures a sufficiently wide electrochemical window for all-solid-state LMBs. From the study of defect configurations and defect formation energies of four types of defects, we find that the interstitial Li ($Li_i^{\bullet}$) and ($V_{Li}^{'} - Li_i^{\bullet}$) Frenkel defect pair are the two most energetically favorable defects with smaller defect formation energies. CI-NEB calculations reveal that the "kick-off" collective migration is the dominant conduction mechanism for $Li_i^{\bullet}$ with an extremely low energy barrier of 0.05 eV. Estimated by the transition state theory, the corresponding $Li_i^{\bullet}$ self-diffusion coefficient is in the order of magnitude of 10^{-3} cm^2/s at room temperature, which demonstrates that the *Pmc2₁* LiGaOS is a promising fast Li-ion conductor.

Data availability

The raw/processed data required to reproduce these findings cannot be shared at this time due to technical or time limitations.

Acknowledgments

The authors thank the National Science Foundation of China (Grant No. 11764019, 11564016, 11664012) for major financial support of the current work. The partial computations were performed on TianHe-1 (A) at the National Supercomputer Center in Tianjin. We would also like to thank US National Science Foundation for supporting this work (NSF-DMR-1801284).

References

[1] M.S. Whittingham, Ultimate limits to intercalation reactions for lithium batteries, Chem. Rev. 114 (23) (2014) 11414–11443.
[2] R. Kanno, M. Murayama, Lithium ionic conductor thio-LISICON: the Li_2S-GeS_2-P_2S_5 system, J. Electrochem. Soc. 148 (7) (2001) A742–A746.
[3] F. Mizuno, A. Hayashi, K. Tadanaga, M. Tatsumisago, New, highly ion-conductive crystals precipitated from Li_2S-P_2S_5 glasses, Adv. Mater. 17 (7) (2005) 918–921.
[4] M. Shoji, E.J. Cheng, T. Kimura, K. Kanamura, Recent progress for all solid state battery using sulfide and oxide solid electrolytes, J. Phys. D Appl. Phys. 52 (10) (2019) 103001.
[5] N. Kamaya, K. Homma, Y. Yamakawa, M. Hirayama, R. Kanno, M. Yonemura, T. Kamiyama, Y. Kato, S. Hama, K. Kawamoto, A. Mitsui, A lithium superionic conductor, Nat. Mater. 10 (9) (2011) 682–686.
[6] S.P. Ong, Y. Mo, W.D. Richards, L. Miara, H.S. Lee, G. Ceder, Phase stability, electrochemical stability and ionic conductivity of the $Li_{10\pm1}MP_2X_{12}$(M = Ge, Si, Sn, Al or P, and X = O, S or Se) family of superionic conductors, Energy Environ. Sci. 6 (1) (2013) 148–156.
[7] P. Bron, S. Johansson, K. Zick, J. Schmedt auf der Gunne, S. Dehnen, B. Roling, $Li_{10}SnP_2S_{12}$: an affordable lithium superionic conductor, J. Am. Chem. Soc. 135 (42) (2013) 15694–15697.
[8] Y. Seino, T. Ota, K. Takada, A. Hayashi, M. Tatsumisago, A sulphide lithium super ion conductor is superior to liquid ion conductors for use in rechargeable batteries, Energy Environ. Sci. 7 (2) (2014) 627–631.
[9] Y. Mo, S.P. Ong, G. Ceder, First principles study of the $Li_{10}GeP_2S_{12}$ lithium super ionic conductor, Material, Chem. Mater. 24 (1) (2011) 15–17.
[10] Z.Q. Wang, M.S. Wu, G. Liu, X.L. Lei, B. Xu, C.Y. Ouyang, Elastic properties of new solid state electrolyte material $Li_{10}GeP_2S_{12}$: a study from first-principles calculations, Int. J. Electrochem. Sc. 9 (2) (2014) 562–568.
[11] C. Yu, S. Ganapathy, E.R.H. van Eck, L. van Eijck, N. de Klerk, E.M. Kelder, M. Wagemaker, Investigation of Li-ion transport in $Li_7P_3S_{11}$ and solid-state lithium batteries, J. Energy Chem. 38 (2019) 1–7.
[12] Y. Sun, X. Zhan, J. Hu, Y. Wang, S. Gao, Y. Shen, Y.T. Cheng, Improving ionic conductivity with bimodal-sized $Li_7La_3Zr_2O_{12}$ fillers for composite polymer electrolytes, ACS Appl. Mater. Interfaces 11 (13) (2019) 12467–12475.
[13] T. Thompson, S. Yu, L. Williams, R.D. Schmidt, R. Garcia-Mendez, J. Wolfenstine, J.L. Allen, E. Kioupakis, D.J. Siegel, J. Sakamoto, Electrochemical window of the Li-ion solid electrolyte $Li_7La_3Zr_2O_{12}$, ACS Energy Lett 2 (2) (2017) 462–468.
[14] P. Zhao, G. Cao, Z. Jin, H. Ming, Y. Wen, Y. Xu, X. Zhu, Y. Xiang, S. Zhang, Self-consolidation mechanism and its application in the preparation of Al-doped cubic $Li_7La_3Zr_2O_{12}$, Mater. Des. 139 (2018) 65–71.
[15] S. Song, D. Sheptyakov, A.M. Korsunsky, H.M. Duong, L. Lu, High Li ion conductivity in a garnet-type solid electrolyte via unusual site occupation of the doping Ca ions, Mater. Des. 93 (2016) 232–237.
[16] Y. Luo, Y. Zhang, Q. Zhang, Y. Zheng, H. Chen, L. Guo, Effect of dual doping on the structure and performance of garnet-type $Li_7La_3Zr_2O_{12}$ ceramic electrolytes for solid-state lithium-ion batteries, Ceram. Int. 45 (14) (2019) 17874–17883.
[17] H.Y. Li, B. Huang, Z. Huang, C.A. Wang, Enhanced mechanical strength and ionic conductivity of LLZO solid electrolytes by oscillatory pressure sintering, Ceram. Int. 45 (14) (2019) 18115–18118.
[18] Y. Zhao, L.L. Daemen, Superionic conductivity in lithium-rich anti-perovskites, J. Am. Chem. Soc. 134 (36) (2012) 15042–15047.
[19] M.S. Wu, B. Xu, X.L. Lei, K. Huang, C.Y. Ouyang, Bulk properties and transport mechanisms of a solid state antiperovskite Li-ion conductor Li_3OCl: insights from first principles calculations, J. Mater. Chem. 6 (3) (2018) 1150–1160.
[20] X. Wang, R. Xiao, H. Li, L. Chen, Oxysulfide LiAlSO, A lithium superionic conductor from first principles, Phys. Rev. Lett. 118 (19) (2017) 195901.
[21] G. Kresse, J. Hafner, Ab initiomolecular dynamics for liquid metals, Phys. Rev. B 47 (1) (1993) 558–561.
[22] G. Kresse, J. Furthmüller, Efficient iterative schemes for ab initio total-energy calculations using a plane-wave basis set, Phys. Rev. B 54 (16) (1996) 11169–11186.
[23] G. Kresse, D. Joubert, From ultrasoft pseudopotentials to the projector augmented-wave method, Phys. Rev. B 59 (3) (1999) 1758–1775.
[24] P.E. Blöchl, Projector augmented-wave method, Phys. Rev. B 50 (24) (1994) 17953–17979.
[25] J.P. Perdew, K. Burke, M. Ernzerhof, Generalized gradient approximation made simple, Phys. Rev. Lett. 77 (18) (1996) 3865–3868.
[26] H.J. Monkhorst, J.D. Pack, Special points for Brillouin-zone integrations, Phys. Rev. B 13 (12) (1976) 5188–5192.
[27] G. Henkelman, B.P. Uberuaga, H. Jónsson, A climbing image nudged elastic band method for finding saddle points and minimum energy paths, J. Chem. Phys. 113 (22) (2000) 9901–9904.
[28] G. Henkelman, H. Jónsson, Improved tangent estimate in the nudged elastic band method for finding minimum energy paths and saddle points, J. Chem. Phys. 113 (22) (2000) 9978–9985.
[29] A. Togo, I. Tanaka, First principles phonon calculations in materials science, Scr. Mater. 108 (2015) 1–5.
[30] X. Gonze, C. Lee, Dynamical matrices, Born effective charges, dielectric permittivity tensors, and interatomic force constants from density-functional perturbation theory, Phys. Rev. B 55 (16) (1997) 10355–10368.
[31] J.E. Saal, S. Kirklin, M. Aykol, B. Meredig, C. Wolverton, Materials design and discovery with high-throughput density functional theory: the open Quantum materials Database (OQMD), JOM (J. Occup. Med.) 65 (11) (2013) 1501–1509.
[32] S. Kirklin, J.E. Saal, B. Meredig, A. Thompson, J.W. Doak, M. Aykol, S. Rühl, C. Wolverton, The Open Quantum Materials Database (OQMD): assessing the accuracy of DFT formation energies, npj Comput. Mater. 1 (1) (2015) 15010.
[33] A.V. Krukau, O.A. Vydrov, A.F. Izmaylov, G.E. Scuseria, Influence of the exchange screening parameter on the performance of screened hybrid functionals, J. Chem. Phys. 125 (22) (2006) 224106.
[34] H.R. Yao, Z.Q. Wang, M.S. Wu, G. Liu, X.L. Lei, B. Xu, J.X. Le, C.Y. Ouyang, Lithium ion migration in Li-Si alloys: from first principles studies, Int. J. Electrochem. Sc. 9 (4) (2014) 1854–1866.
[35] W. Xia, B. Xu, H. Duan, Y. Guo, H. Kang, H. Li, H. Liu, Ionic conductivity and air stability of Al-doped $Li_7La_3Zr_2O_{12}$ sintered in alumina and Pt crucibles, ACS Appl. Mater. Interfaces 8 (8) (2016) 5335–5342.
[36] H. Buschmann, J. Dolle, S. Berendts, A. Kuhn, P. Bottke, M. Wilkening, P. Heitjans, A. Senyshyn, H. Ehrenberg, A. Lotnyk, V. Duppel, L. Kienle, J. Janek, Structure and dynamics of the fast lithium ion conductor "$Li_7La_3Zr_2O_{12}$, Phys. Chem. Chem. Phys. 13 (43) (2011) 19378–19392.
[37] M. Monchak, T. Hupfer, A. Senyshyn, H. Boysen, D. Chernyshov, T. Hansen, K.G. Schell, E.C. Bucharsky, M.J. Hoffmann, H. Ehrenberg, Lithium diffusion pathway in Li(1.3)Al(0.3)Ti(1.7)(PO4)3 (LATP) superionic conductor, Inorg. Chem. 55 (6) (2016) 2941–2945.
[38] C. Ouyang, L. Chen, Physics towards next generation Li secondary batteries materials: a short review from computational materials design perspective, Sci. China Phys. Mech. 56 (12) (2013) 2278–2292.
[39] G.H. Vineyard, Frequency factors and isotope effects in solid state rate processes, J. Phys. Chem. Solids 3 (1957) 121–127.
[40] C.H. Hu, Z.Q. Wang, Z.Y. Sun, C.Y. Ouyang, Insights into structural stability and Li superionic conductivity of $Li_{10}GeP_2S_{12}$ from first-principles calculations, Chem. Phys. Lett. 591 (2014) 16–20.